



# Valorization of Silicomanganese Slag into Reusable Porous High-Performance Nanosilica for Recovery of Water from Methylene Blue Wastewater

Morteza Namvar<sup>1</sup> · Mostafa Mahinroosta<sup>1</sup> · Ali Allahverdi<sup>1</sup>

Received: 20 July 2022 / Accepted: 20 November 2022 / Published online: 6 December 2022  
© The Minerals, Metals & Materials Society 2022

## Abstract

The conversion of industrial wastes into advanced materials with environmental applications has always been one of the fascinating and promising research topics. This study investigates the removal of methylene blue dye using porous nanosilica obtained from silicomanganese slag. First, porous nanosilica was obtained from the silicomanganese slag using a facile and high-efficiency waste valorization path. The valorization path exhibited a dissolution efficiency of more than 96%. The obtained nanosilica possessed a specific surface area and total pore volume of 506 m<sup>2</sup>/g and 0.65 cm<sup>3</sup>/g, respectively, with the peak pore size of around 10 nm. The obtained nanosilica was then used to adsorb methylene blue dye from aqueous solutions. The results showed that a 96–98% dye adsorption efficiency could be achieved under the adsorbent dosage of 0.4 g/L, pH 7, contact time = 60 min, and ambient temperature. Fitting the isotherm models revealed that the Langmuir model could better predict the experimental adsorption data, meaning monolayer adsorption occurred. The maximum dye adsorption capacity of the porous nanosilica obtained from the Langmuir model constant was 256.41 mg/g. Also, the pseudo-second-order kinetic model could better fit the adsorption data, which meant the chemisorption of the dye on the adsorbent surface. Dye adsorption on the adsorbent microstructure was also confirmed by energy-dispersive X-ray spectroscopy, elemental mapping, and Fourier-transform infrared spectroscopy analyses. The reusability experiments indicated that the porous nanosilica could exhibit removal efficiency of higher than 90% until the fourth reuse. The overall results showed that by converting silicomanganese slag into an adsorbent with high dye removal performance, both a solution for slag management and dye removal from effluents could be proposed. These two paths can help to create a cleaner environment.

---

The contributing editor for this article was Zhi Sun.

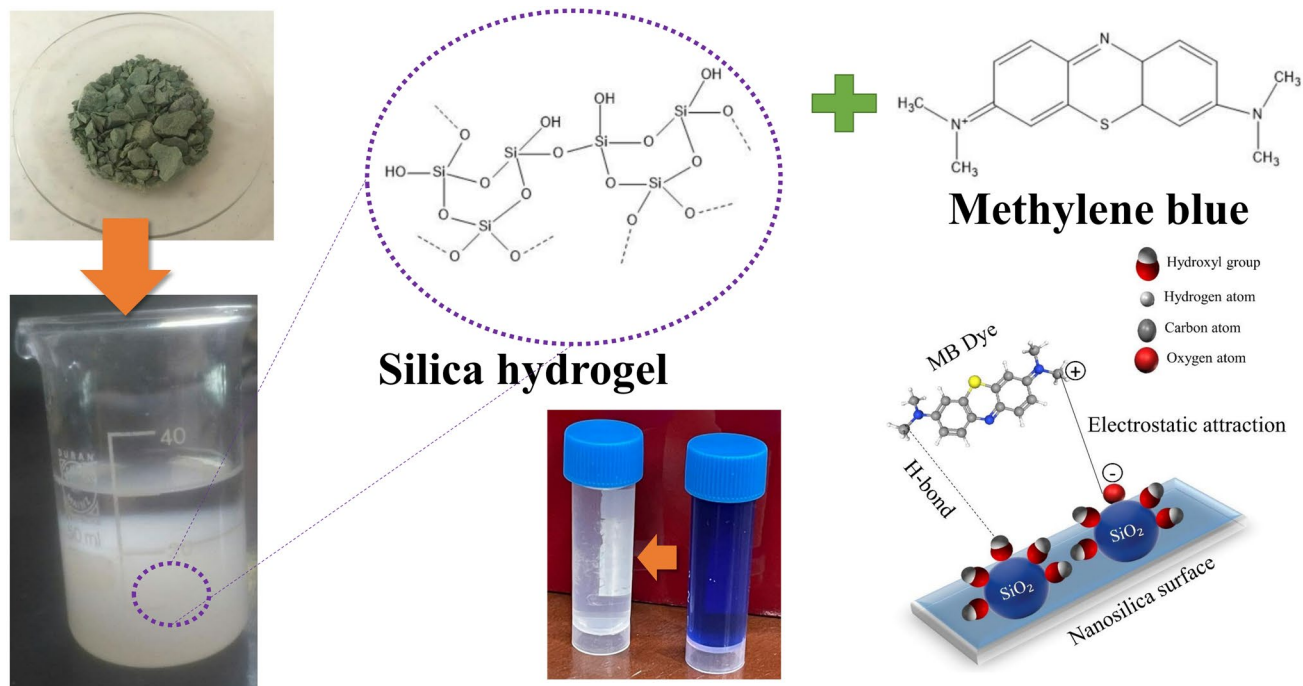
✉ Mostafa Mahinroosta  
mahinroosta2010@gmail.com

✉ Ali Allahverdi  
ali.allahverdi@iust.ac.ir

Morteza Namvar  
morteza.namvar72@gmail.com

<sup>1</sup> Research Laboratory of Inorganic Chemical Process Technologies, School of Chemical Engineering, Iran University of Science and Technology, Narmak, Tehran 1684613114, Iran

## Graphical Abstract



**Keywords** Dye · Slag · Nanosilica · Adsorption · Waste recycling

## Introduction

In recent years, the population growth and industrial activities of human beings are associated with excessive consumption in all areas. This unbridled increase has caused not only the majority of people in parts of the world to suffer from a deficiency of freshwater sources [1–3], but also large volumes of pollutants entering the ecosystem [4, 5]. Meanwhile, water pollution due to its long-term effects is one of the most critical issues in the world today [6]. Chemical dyes and pigments that are directly correlated with the various industries such as paper, textile, rubber, tannery, plastics, and cosmetics are among the most important causes of water pollution because they elicit changes in the natural appearance of water even at deficient concentrations [7–9]. The presence of dye pollutants in the environment is hazardous for human health, leading to skin and mucosal diseases and even leading to cancer [10]. It is estimated that an enormous volume of almost 700,000 tons of dye-stuff is generated annually [11–13]. Therefore, managing and reducing dye pollution is one of the most important issues globally, and many researchers have studied the possible solutions in this field.

During the last decades, various techniques, such as physical, chemical, and biological methods, have been

used to remove dyes from aqueous solutions [14]. Among the numerous methods developed, adsorption is one of the most effective ways to remove these dyes from wastewater due to its efficiency and cost-effectiveness [14]. Therefore, there are several studies in which silica, activated carbon, glass hollow fiber, kaolinite, zeolites, mesoporous magnetic silica composite, organic hybrid super-microporous silica, ash, mucuna beans, rice husk, cow dung, sludge biochar,  $\text{MgFe}_2\text{O}_4$ /reduced graphene oxide, microcrystalline cellulose from oil palm fronds, walnut shells powder, and carbon nanofibers from polyacrylonitrile have been used as the dye adsorbent [15–27].

In recent studies, mesoporous nanosilica [28], biogenic zirconium oxide nanoparticles [29], and ternary nanocomposite aerogel [30] have been used to adsorb methylene blue under different test conditions. The main challenges of these studies include the unavailability and high price of precursors or raw materials for large-scale adsorbent production, long contact times, high temperatures, and alkaline pHs.

Therefore, remediating dye-polluted water by widely available low-cost adsorbent from industrial wastes can help to reduce health risks to the community and environmental problem. Recovery of precious elements from secondary resources has gained renewed interest as an environmentally

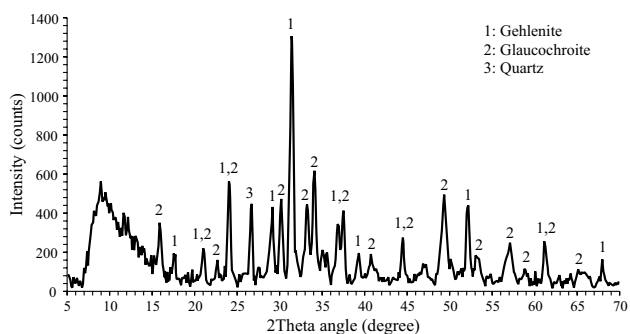
**Table 1** Oxide composition of the silicomanganese slag

Oxide	SiO <sub>2</sub>	CaO	Al <sub>2</sub> O <sub>3</sub>	MnO	MgO	Fe <sub>2</sub> O <sub>3</sub>	K <sub>2</sub> O
Wt%	38.17	29.30	14.78	10.29	2.77	0.76	0.42

friendly option and caused productive avail excess in wastewater treatment to access to clean drinking water [1–3].

As mentioned above, the sources used to prepare the adsorbents can be divided into three categories: primary sources, secondary sources or wastes, and analytical-grade precursors. These adsorbents have exhibited a dye removal efficiency of about 80 to 99% and an adsorption capacity of 10 to 178 mg/g under different adsorption test conditions. In addition, the use of analytical-grade precursors to produce large-scale adsorbents is challenging and may adversely affect the economics of the adsorption process. Therefore, producing an effective adsorbent from an inexpensive source is always an essential requirement, especially when treating high amounts of colored effluent. In addition to the above, producing an adsorbent from a secondary source (such as an industrial waste) can have several advantages. First, natural resources return to the use cycle and are prevented from being wasted. Second, the volume of waste accumulation in the environment and the resulting pollution are reduced. Third, converting waste into a valuable material with environmental applications can lead to economic benefits and a cleaner environment.

This study uses low-cost, highly pure porous nanosilica synthesized from silicomanganese slag as an efficient and reusable adsorbent for methylene blue removal from aqueous solutions. Also, the effects of initial dye concentrations, contact time, solution pH, and amount of adsorbent on the dye removal performance are investigated.

**Fig. 1** XRD pattern of silicomanganese slag [28] (with kind permission from Elsevier)

## Materials and Methods

### Materials

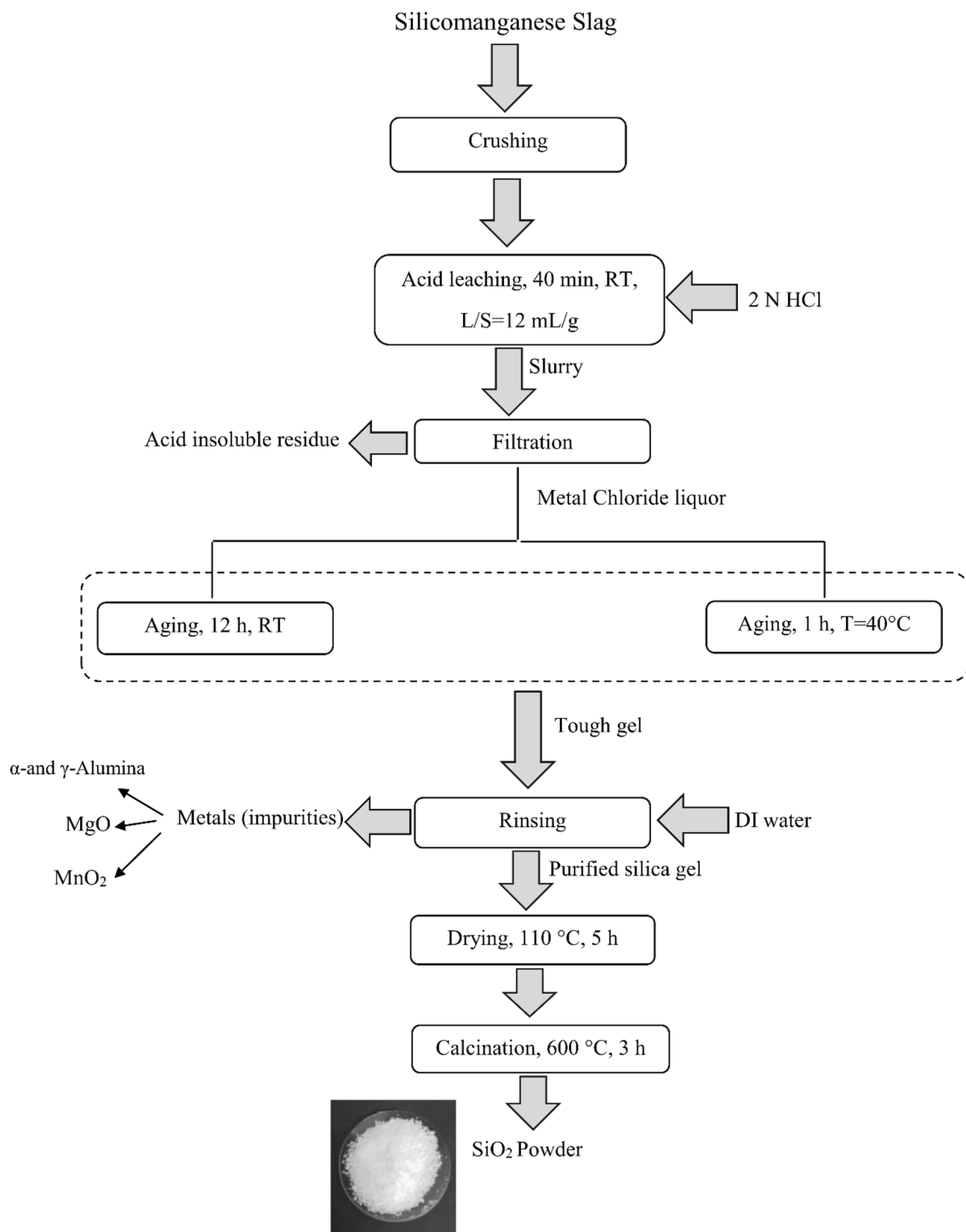
The silicomanganese slag (SMS) used in this study was provided from the Faryab ferro-alloy manufacturing plant located in Hormozgan province in Iran. More than 15,000 tons of SMS are annually generated and gathered in the plant space [31]. The received SMS pile was ground into small granules. The chemical composition of the SMS is presented in Table 1. As presented in Table 1, it consists chiefly of SiO<sub>2</sub>, CaO, Al<sub>2</sub>O<sub>3</sub>, and MnO along with other oxides.

Figure 1 depicts the X-ray diffractogram of the SMS, indicating the presence of three major crystalline phases of gehlenite (Ca<sub>2</sub>Al<sub>2</sub>SiO<sub>7</sub>), glaucocroite ((Ca, Mn)<sub>2</sub>SiO<sub>7</sub>), and quartz (SiO<sub>2</sub>).

Methylene blue with dye contents of 82%, hydrochloric acid (HCl, 37%), and sulfuric acid (H<sub>2</sub>SO<sub>4</sub>, 96–98%) were

**Table 2** Dissolution experiments were conducted at different conditions

Test No	Liquid-to-solid ratio (mL/g)	Hydrochloric acid concentration (N)	Dissolution time (min)	Dissolution temperature (°C)
1	120	2	40	RT
2	120	3	60	60
3	120	7	20	30
4	60	7	40	50
5	60	3	60	RT
6	60	9	20	40
7	60	0.5	40	30
8	30	2	15	40
9	30	9	20	60
10	30	1	60	RT
11	12	2	40	RT
12	12	5	60	50
13	12	2	15	60
14	7.5	7	15	30
15	7.5	11	40	RT
16	7.5	5	60	40
17	6	9	10	40
18	6	7	60	30
19	6	11	20	RT
20	4	11	20	40
21	4	5	60	RT
22	4	9	40	60



**Fig. 2** Synthesis pathway of silica nanopowder from silicomanganese slag (RT: room temperature)

supplied from Merck (Darmstadt, Germany), and pellet sodium hydroxide (NaOH, 98%) was purchased from Daejung Chemicals (South Korea). Deionized water was used for the preparation of aqueous solutions.

## Methods

### Synthesis of Porous Nanosilica

At the first step for optimal extraction of silica from the SMS, the dissolution tests were performed by aqueous

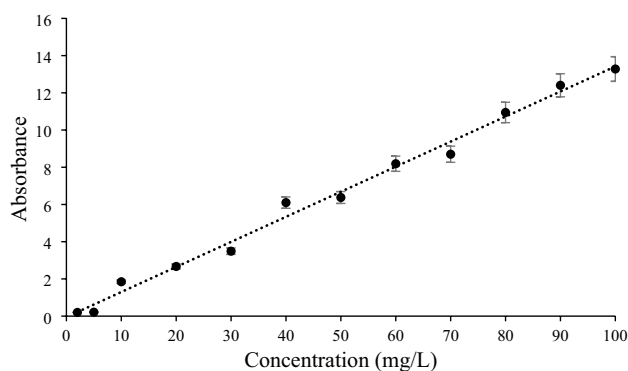


**Fig. 3** Calibration curve for converting the absorbance values to methylene blue concentration

solutions of NaOH, HCl, and H<sub>2</sub>SO<sub>4</sub> under same conditions. The primary results revealed that HCl could exhibit a higher dissolution efficiency than NaOH and H<sub>2</sub>SO<sub>4</sub>. The dissolution efficiencies achieved by NaOH, HCl, and H<sub>2</sub>SO<sub>4</sub> were ~39%, 92%, and ~41%, respectively. Then, the effect of various process parameters including liquid-to-solid ratio, temperature, dissolution time, and HCl concentration on the dissolution efficiency was investigated. For this purpose, dissolution experiments were conducted at different conditions (as presented in Table 2).

Figure 2 depicts the various operations involved in the extraction of silica gel from the SMS. The porous nanosilica synthesis process consisted of four stages, including acid leaching, filtration, aging, and purification. As a typical synthesis process, 5 g of the SMS was transferred to a glass reactor containing 60 mL of 2 N HCl dissolving agent at room temperature and stirred for 40 min. The obtained slurry was then filtered using Whatman filter paper to separate the acid-insoluble residue from the achieved silicic acid/metal chloride mixture. The mixture was aged 12 h at room temperature or heated at 40 °C for 1 h until a tough gel emerged, having a pale green color. The achieved gel was rinsed with deionized water several times to remove any metal chloride impurities (i.e., CaCl<sub>2</sub>, MnCl<sub>2</sub>, AlCl<sub>3</sub>, MgCl<sub>2</sub>, etc.). The rinsed gel was dried at 105 °C and then calcined at 600 °C for 3 h.

### Water Recovery Experiments

At first, a 100 mg/L stock solution was prepared by dissolving an appropriate quantity of methylene blue in deionized water. The dye solutions with the lower concentrations were obtained by diluting the stock solution. All batch adsorption experiments were conducted at ambient temperature (25 °C). The dye adsorption tests were performed in a 100-mL glass beaker containing 50 mL of the methylene blue solution. A specific dosage of adsorbents was added to the various

concentrations of methylene blue solution under stirring conditions at 140 rpm. The porous nanosilica was separated via paper filtration at the end of the adsorption period. The concentration of methylene blue solutions was determined using a UV–Visible spectrophotometer at  $\lambda_{\max}$  of 663 nm. A calibration curve was obtained to convert the absorbance values to mg/L, which is shown in Fig. 3.

The effects of several factors such as initial methylene blue concentration (20–100 mg/L), initial pH of dye solutions (2–12), the contact time (5–120 min), and adsorbent amount (0.1–0.5 g) were investigated. The pH of the dye solutions was adjusted by adding 0.1 mol/L NaOH or 0.1 mol/L HCl.

The amounts of methylene blue adsorbed on porous nanosilica hydrogel at any time were calculated using Eq. (1):

$$q_t = V(C_0 - C_e)/W. \quad (1)$$

in which  $q_t$  (mg/g) is the amount of methylene blue adsorbed,  $C_0$  and  $C_{eq}$  (mg/L) are the initial and equilibrium liquid phase concentrations, respectively,  $V$  (L) is the volume of the dye solution, and  $W$  (g) is the adsorbent mass.

The dye removal percentage was calculated by Eq. (2):

$$\% \text{Removal} = [(C_0 - C_e)/C_0] \times 100. \quad (2)$$

### Adsorption Isotherms

The adsorption isotherm provides knowledge about the nature of the adsorption process and the adsorption capacity of the adsorbent. Langmuir and Freundlich isotherm models are the most widely accepted isotherms to determine the relationship between the amount of the adsorbate and the equilibrium concentration of an adsorptive solution [32].

The Langmuir and Freundlich isotherm models were used to test the experimental equilibrium data for the adsorbed methylene blue on the porous nanosilica hydrogel. The well-known expression of the Langmuir model is as follows [33–35]:

$$1/q_e = 1/Kq_{\max} \cdot 1/C_e + 1/q_{\max}, \quad (3)$$

in which  $q_e$  (mg/g) is the amount of methylene blue adsorbed at the equilibrium,  $C_e$  (mg/L) is the methylene blue concentration at the equilibrium,  $q_{\max}$  (mg/g) is the maximum adsorption capacity of the methylene blue, and  $K$  is the Langmuir constant that described the free energy of the adsorption. The values of  $q_{\max}$  and  $k$  could be directly computed from the intercept and the slope of the linear plot of  $1/q_e - 1/C_e$ . The applicability of the Langmuir isotherm is expressed by the equilibrium parameter,  $R_L$  [33–35]:

$$R_L = 1/(1 + KC_0). \quad (4)$$

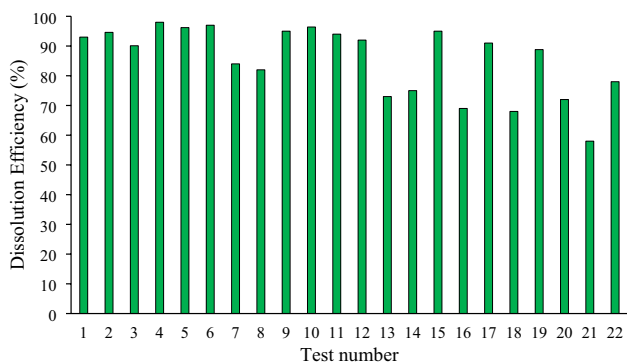


**Fig. 4** Silicomanganese slag dissolution efficiency under different conditions

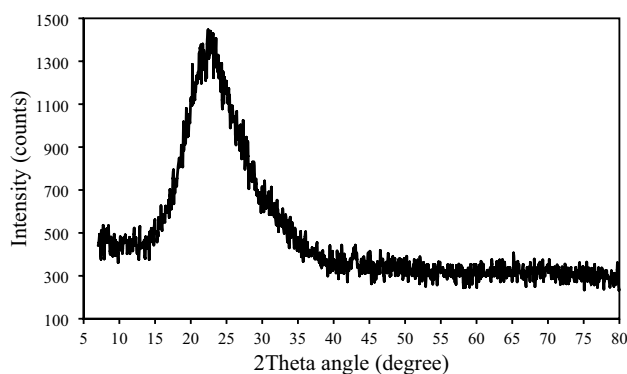


**Fig. 5** XRD pattern of the synthesized porous nanosilica

The values of  $0 < R_L < 1$  represent a favorable adsorption, while  $R_L = 0,1$  and  $R_L > 1$  indicate an irreversible and an unfavorable adsorption, respectively.

The Freundlich equation is expressed as

$$\text{Log}q_e = \text{Log}K_f + 1/n\text{Log}C_e. \tag{5}$$

In this model,  $K_f$  (mg/g) and  $n$  express the adsorption capacity of adsorbent and adsorbent affinity to adsorbate, respectively.

**Adsorption Kinetics**

Kinetics study is used to describe the rate-controlling step and the methylene blue adsorption process mechanism. In this work, to study the adsorption kinetics of methylene blue on microporous nanosilica hydrogel, three kinetics models,

namely the pseudo-first-order, pseudo-second-order, and intraparticle diffusion, were applied to fit the adsorption data. The pseudo-first-order model is as follows [33–35]:

$$\log (q_e - q_t) = \log q_e - k_1 t, \tag{6}$$

where  $k_1$  ( $\text{min}^{-1}$ ) is the equilibrium rate constant, and  $q_e$  and  $q_t$  correspond to the methylene blue adsorption quantity (mg/g) at equilibrium and time  $t$ , respectively. The pseudo-second-order equation is as follows [33–35]:

$$t/q_t = 1/K_2q_e^2 + t/q_t, \tag{7}$$

where  $K_2$  (g/mg min) is the rate constant.

The intraparticle diffusion model is expressed according to Eq. (8) [33–35]:

$$q_t = K_{di}t^{0.5} + C_i, \tag{8}$$

where  $C_i$  is the y-intercept of the plot (mg/g), and  $K_{di}$  is the intraparticle diffusion rate ( $\text{mg}/\text{min}^{1/2} \text{g}$ ).

**Statistical Parameters**

When the correlation factors,  $R^2$ , of the fitted models are close to each other, the validity of the models should be confirmed by nonlinear statistics, such as the chi-square test ( $\chi^2$ ). The following equation can express the nonlinear chi-square test:

$$\chi^2 = \sum (y_{\text{exp}} - y_{\text{cal}})^2 / y_{\text{cal}}, \tag{9}$$

where  $y_{\text{exp}}$  and  $y_{\text{cal}}$  are the experimental and predicted data by model, respectively. Based on Eq. (9), a model can better fit experimental data with the lowest  $\chi^2$  value.

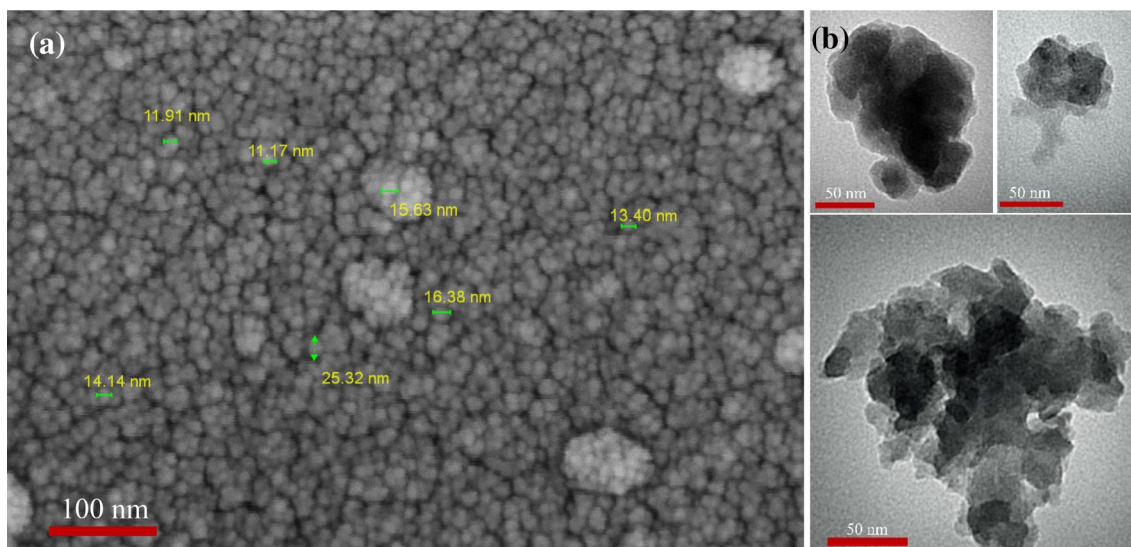
**Reusability Experiments**

To investigate the reusability of the synthesized porous nanosilica, a bunch of adsorption experiments was carried out using the porous nanosilica. For reusability experiments, 0.4 g/L of the porous nanosilica was added to 50 mL of methylene blue solution with concentration of 20 mg/L at pH 7, and stirred for 60 min under room temperature. The solution was filtered using Whatman filter paper to separate the adsorbent for another consecutive cycle, without the desorption stage.

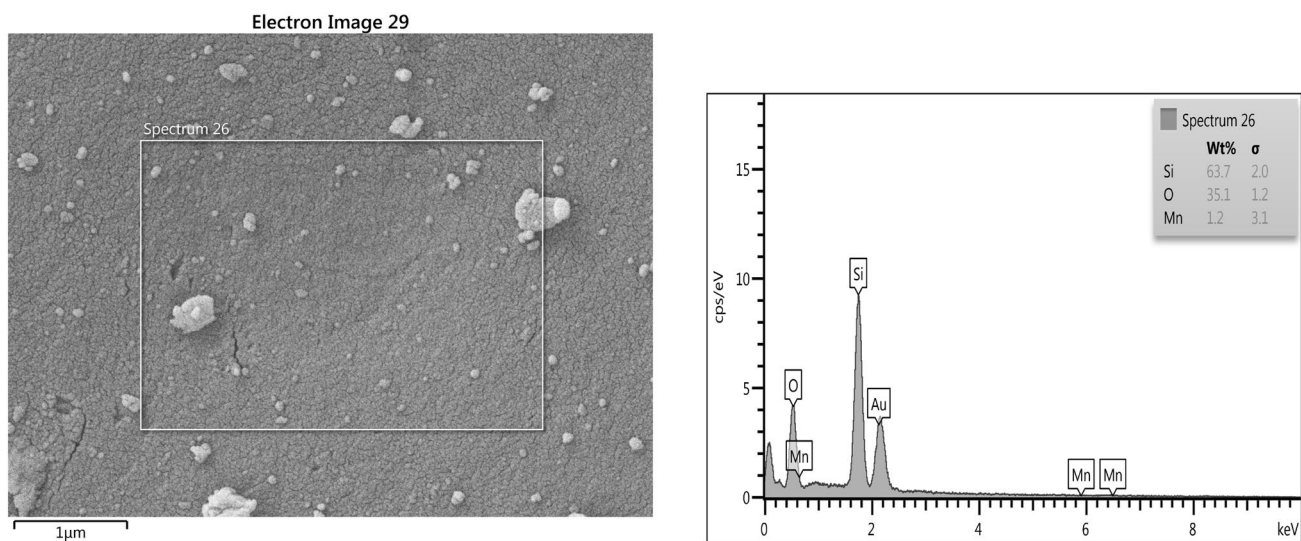
**Table 3** XRF chemical composition of the extracted microporous nanosilica

Oxide	SiO <sub>2</sub>	CaO	Al <sub>2</sub> O <sub>3</sub>	MgO	Fe <sub>2</sub> O <sub>3</sub>	K <sub>2</sub> O	Na <sub>2</sub> O
Wt%	99.08	0.014	0.012	0.021	0.025	0.038	0.02



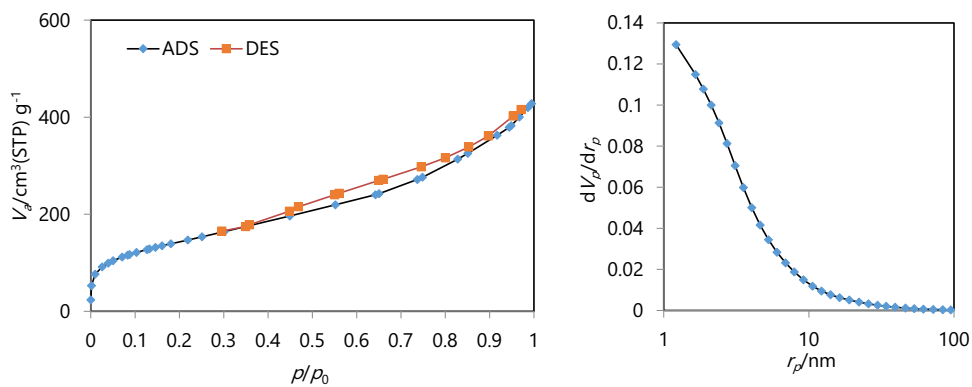


**Fig. 6** a FESEM and b TEM images of the synthesized porous nanosilica



**Fig. 7** EDS spectrum of the extracted nanosilica

**Fig. 8** (Left) the BJH-adsorption pore size distribution, (Right)  $N_2$  adsorption–desorption data of the prepared mesoporous nanosilica



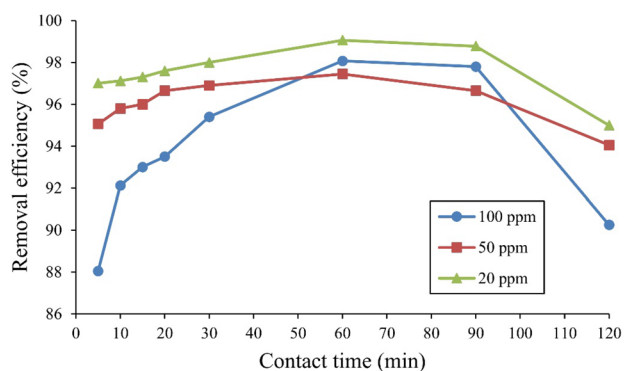


**Fig. 9** Effect of contact time and initial concentration on the removal efficiency of methylene blue (pH  $6 \pm 0.2$ , adsorbent dosage = 0.4 g/L, room temperature)

### Characterization Techniques

The mineralogical study of porous nanosilica hydrogel was performed by X-ray diffractometer, using a Philips Expert System at 40 kV and 30 mA. The XRD test was prepared at  $2\theta$  range of  $5^\circ$ – $80^\circ$  with a scanning rate of  $2^\circ/\text{min}$ , anti-scatter, and receiving slit of  $1^\circ$  and 0.01 mm, respectively. The chemical composition of the synthesized porous nanosilica was found using a Philips PW1480 X-ray fluorescence (XRF) analyzer (ASTME1621 standard). The microstructure of porous nanosilica particles was investigated using ZEISS field emission scanning electron microscope (FESEM) (SIGMA VP-500, Germany) at a voltage of 15 kV and the elemental analysis was carried out by Energy-Dispersive X-ray (EDX) detector (Oxford Instrument, England). TEM analysis was recorded with a PHILIPS CM12 (Netherlands) microscope operating at 120 kV. The specific surface area was determined by BET isotherm using  $N_2$  at 77 K (BEISORP Mini). In order to identify the involvement of

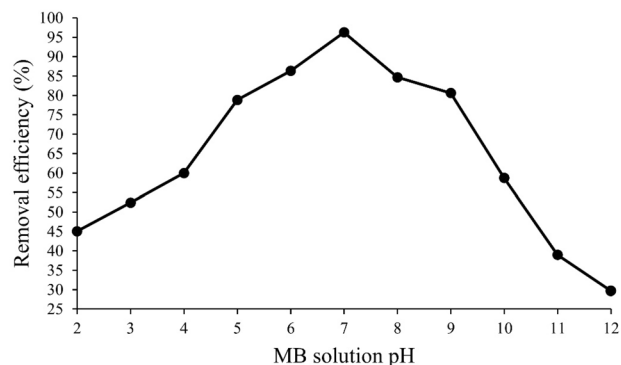


**Fig. 10** Effect of different pH values on methylene blue dye adsorption (adsorbent dosage = 0.4 g/L, contact time = 60 min, room temperature, concentration = 20 mg/L)

different functional groups of the adsorbent, Fourier-transform infrared spectroscopy (FTIRs) was conducted using a SHIMADZU (IR Spectrophotometer 8400 s) FTIR spectrometer in transmittance mode. All spectra were recorded with a sensitivity of  $4 \text{ cm}^{-1}$  and 64 scans per spectrum. The concentration of methylene blue dye in the liquid phase was analyzed by UV–Vis spectrophotometer (LAMBDA 365 UV).

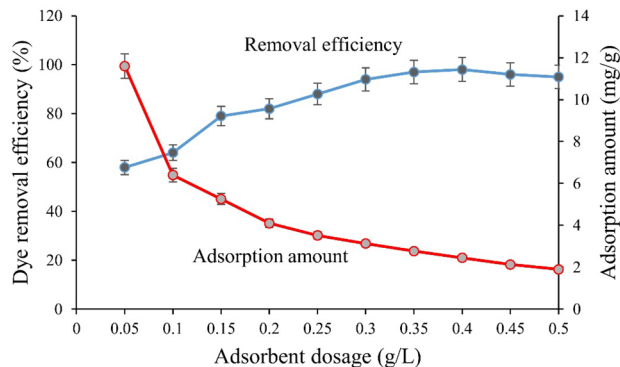
## Results and Discussion

### Dissolution Efficiency and Characterization of Adsorbent

The results of SMS dissolution under different conditions presented in Table 2 are depicted in Fig. 4. It can be seen that in tests 5, 4, and 11, a dissolution efficiency of higher than 96% could be achieved. Test 4 has the highest dissolution efficiency (98%), but consumes a lot of acid. Test 11 with a dissolution efficiency of about 96% has 10 times less acid consumption than the acid consumption of test 4, and therefore, the operating conditions used in test 11 are a good choice for the SMS processing. The XRD pattern of the porous nanosilica synthesized from the SMS is depicted in Fig. 5. As it is evident, the XRD pattern displays a broad hump in the  $2\theta$  values of  $15^\circ$  to  $30^\circ$ , confirming the amorphous structure of the synthesized porous nanosilica [36].

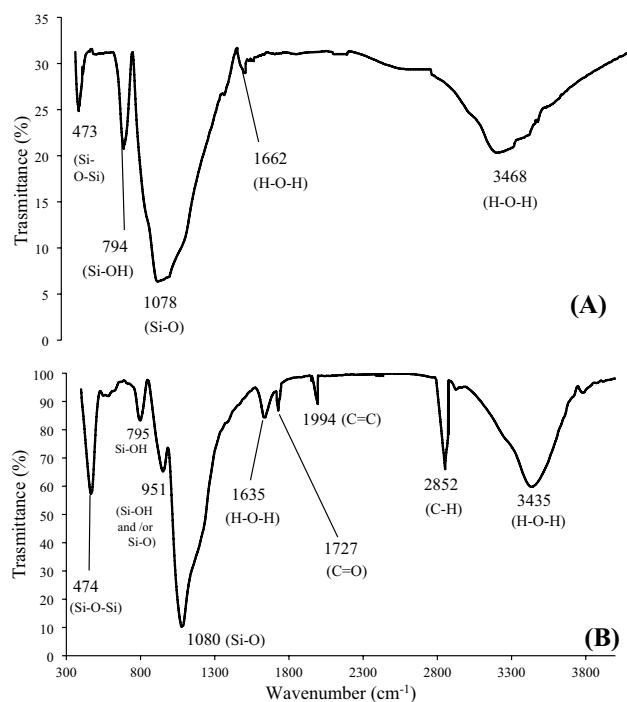
Table 3 presents the XRF chemical composition of the synthesized porous nanosilica. As can be seen in Table 3, the synthesized porous nanosilica contains a high purity of more than 99%. It could be inferred that the other oxides reported are present in tiny amounts of less than 3%.

Figure 6a and b illustrates the FESEM micrograph and TEM images of the porous nanosilica synthesized from the SMS, respectively. From Fig. 6a, a large number of particles



**Fig. 11** Removal efficiency and adsorption amount of methylene blue by porous nanosilica (adsorbent dosage pH 7, Initial dye concentration = 20 mg/L, contact time = 60 min)





**Fig. 12** FTIR spectra of the porous nanosilica before (A) and after (B) methylene blue adsorption

in the size range of 10 to 30 nm are seen. Agglomerates with a size of about 50–70 nm are also observed. The TEM images shown in Fig. 6b confirm that silica agglomerates comprise ~50-nm particles. The porous nanosilica particles are composed of flaky and rounded-corners morphologies.

Figure 7 exhibits the EDS analysis to check the elemental composition of the extracted porous nanosilica. According to the EDS analysis, Si and O were as major components (98.8 wt%) of the extracted porous nanosilica. There was slight amount of Mn in the EDS measurement, which was addressed to chemical composition of starting SMS.

Figure 8 presents nitrogen sorption isotherm and pore size distribution of the prepared porous nanosilica. As can be seen, the results fit the type IV adsorption isotherm with a hysteresis loop in accordance with IUPAC classification. This type of isotherm describes the nature of mesoporous materials. According to the evaluation by the BET method, the value of surface area and pore volume of the extracted nanosilica were 506.14 m<sup>2</sup>/g and 0.65 cm<sup>3</sup>/g, respectively. As seen from Fig. 8, the peak pore size according to the Barrett–Joyner–Halenda (BJH) method is around 10 nm, which proved the formation of a mesoporous structure in the extracted nanosilica.

### Effect of Contact Time and Initial Concentration of Methylene Blue Dye

The effect of various contact times on methylene blue adsorption by the porous nanosilica adsorbent was investigated at an adsorbent dosage of 0.4 g/L, with different initial MB concentrations (with 20, 50, and 100 mg/L, room temperature, and pH 6 ± 0.2). The results are depicted in Fig. 9. As can be seen, the MB removal rate at concentrations of 20 and 50 mg/L is so high that in the first 10 min of contact time, the MB removal efficiency is more than 95%. For an initial concentration of 20 mg/L, with increasing contact time from 5 to 60 min, the removal efficiency increases by only ~2%, from 97.0 to 99.0%. For an initial concentration of 50 mg/L, the removal efficiency increases from 95.0 to 97.4% by increasing the contact time from 5 to 60 min. For an initial concentration of 100 mg/L, the MB removal rate is slower, so that removal efficiency of about 98.0% is achieved after a contact time of 60 min. As contact time increases, more active sites on the adsorbent surface become involved in the dye adsorption process [37]. From Fig. 9, a contact time of 60 min could be considered the equilibrium contact time for all three MB concentrations tested.

### Effect of pH

The effect of MB solution pH that is one of the important influencing parameters for the adsorption of methylene blue onto microporous nanosilica was investigated by varying initial MB solution pH. The experiments were obtained under contact time of 60 min and an adsorbent dosage of 0.4 g/L. The results are depicted in Fig. 10. As shown, by increasing the pH from 2 to 7, the removal efficiency of methylene blue increases dramatically from ~45 to ~96.2%, and by further increasing the pH up to 12, the removal efficiency of methylene blue decreases from ~96.2 to ~29.7%. It was found that a maximum MB removal efficiency of 96.2% on porous nanosilica was achieved at pH 7.

At low pH values, the MB removal efficiency is low. This may be due to the competition of H<sup>+</sup> ions with dye molecules to capture adsorption sites on the adsorbent surface. The excess H<sup>+</sup> ions react with the polar groups of Si–OH on the nanosilica surface, thus occupying the adsorbent surface [38]. At pH > p*H*<sub>pzc</sub> = 3.2, the surface of nanosilica particles is negatively charged, thus an electrostatic attraction is established between the cationic molecules of the dye and the negative surface of the adsorbent. This increases the dye removal efficiency. At pH > 7, the excess OH<sup>−</sup> ions bind to the cationic molecules of the dye to form the MB–OH, which prevents the adsorption of the dye molecules on the adsorbent surface [38].

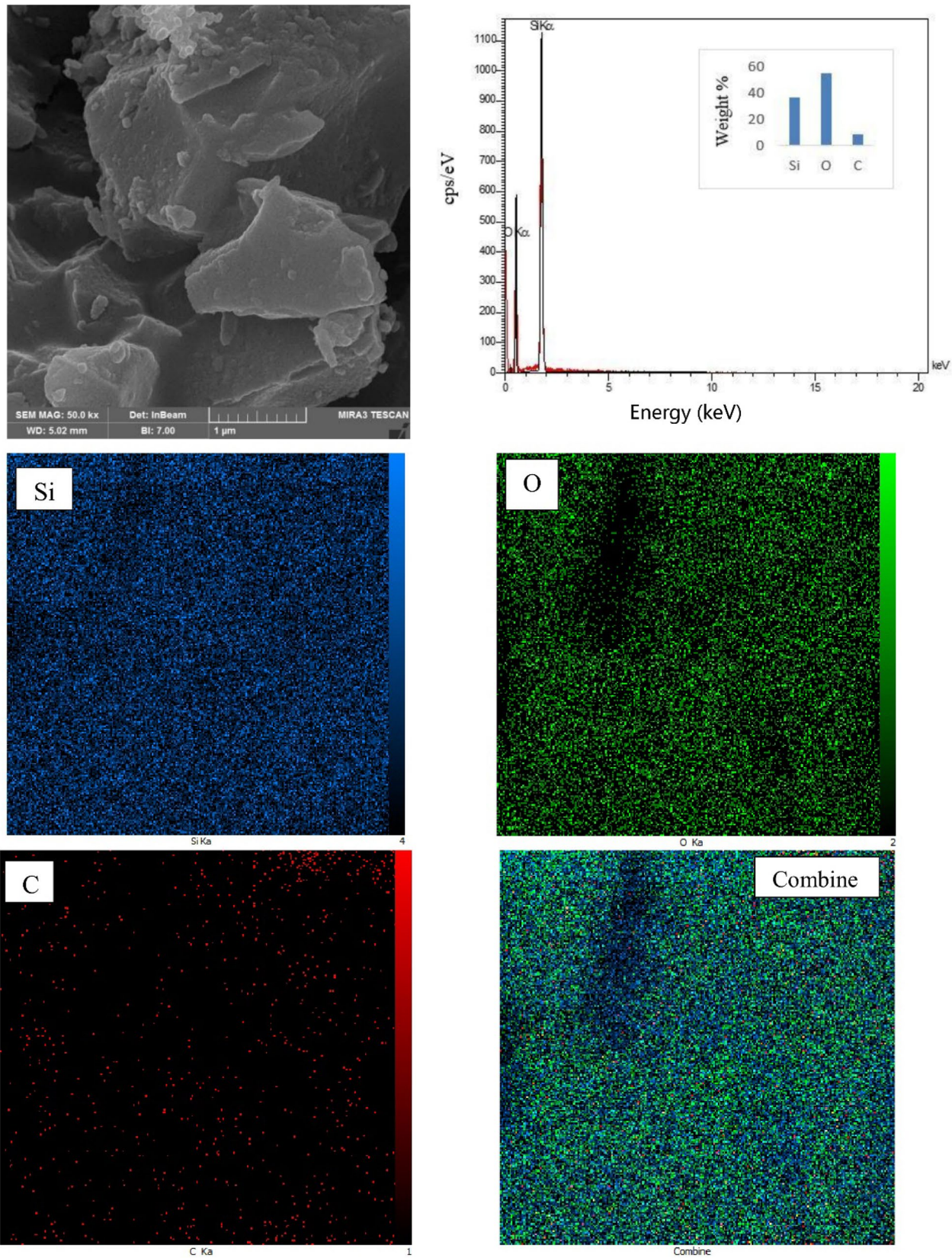
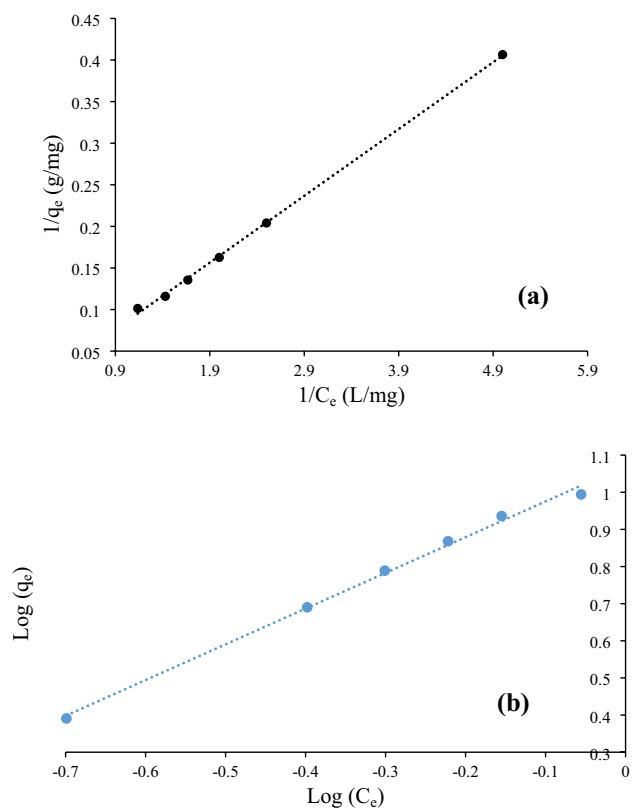


Fig. 13 FESEM image, SEM elemental mapping, and elemental analysis of porous nanosilica after MB adsorption



**Fig. 14** Adsorption isotherms, **a** Langmuir and **b** Freundlich for methylene blue adsorption by microporous nanosilica (pH 7, adsorbent dosage = 0.4 g/L, contact time = 60 min, room temperature)

### Influence of Adsorbent Dosage

The influence of adsorbent dosage on the dye adsorption was investigated at initial MB concentration = 20 mg/L, pH 7, and the contact time = 60 min. The obtained results are presented in Fig. 11. It can be seen from Fig. 11 that the percentage of dye removal increased sharply from 58 to 98% with increasing porous nanosilica amount from 0.05 to 0.4 g/L. This fact can be attributed to the increased sorption sites [39]. Increasing the adsorbent dosage beyond 0.4 g/L caused a decrease in uptake efficiency that can be attributed to the reduction in the effective surface area. Besides, the adsorption amount was decreased from 11.6 to 1.9 mg/g with a rise in the adsorbent dosage from 0.05 to 0.5 g/L. This may be attributed to overlapping adsorption sites due to the decline in the number of binding sites [40]. Maximum

removal of 98% was achieved at the adsorbent dosage of 0.4 g/L.

### Fourier-Transform Infrared Spectroscopy

Figure 12 depicts the FTIR spectra of the porous nanosilica before and after adsorption of the methylene blue dye. The bands located at 473 and 474  $\text{cm}^{-1}$  can be attributed to the Si–O–Si asymmetric stretching vibration. The band at 795  $\text{cm}^{-1}$  belongs to the symmetric stretching of Si–OH. The weak band at 951  $\text{cm}^{-1}$  can be related to Si–OH and /or Si–O<sup>−</sup> groups. The absorption bands at 1078 and 1080  $\text{cm}^{-1}$  can be related to the stretching vibration of Si–O. The vibrational bands at 1635, 1642, 3435, and 3450  $\text{cm}^{-1}$  correspond to the stretching and bending vibrations of H–O–H [41, 42]. The absorption band at 2852  $\text{cm}^{-1}$  indicates the stretching vibration of C–H. The bands at 1994 and 1727 are assigned to the asymmetric stretching of C=C and C=O, respectively [43, 44].

### Microstructural Studies

Figure 13 depicts FESEM image, the energy-dispersive X-ray spectroscopy (EDS) elemental analysis, and the elemental mapping of the porous nanosilica after the adsorption of the methylene blue dye. The EDS elemental analysis confirmed the presence of Si, O, and C. The presence of C is due to the adsorption of the MB dye. The corresponding elemental mapping further emphasized the distribution of Si, O, and C in the porous nanosilica microstructure.

### Adsorption Isotherm

The adsorption isotherms of methylene blue on the porous nanosilica are illustrated in Fig. 14. As seen in Table 4, the high correlation coefficients ( $R^2 = 0.99$ ) indicate that both Langmuir and Freundlich isotherms may be suitable for fitting equilibrium adsorption data. Therefore, nonlinear chi-2 statistic was used to find the best fit. Chi-2 values showed that the Langmuir isotherm model can better fit the experimental equilibrium data. The Langmuir adsorption isotherm demonstrates the occurrence of monolayer adsorption on the adsorbent surface with a limited number of similar sites [45]. According to the Langmuir model, the maximum adsorption capacity calculated for the microporous nanosilica was 256.41 mg/g. The Langmuir isotherm validity was examined by the dimensionless separation parameter,  $R_L$ . In the present

**Table 4** Isotherm parameters for methylene blue adsorption by the porous nanosilica

Langmuir constants				Freundlich constant			
$Q_{\max}$ (mg/g)	$K$ (L/mg)	$R^2$	$\chi^2$	$K_f$ (mg/g)	$n$	$R^2$	$\chi^2$
256.41	0.048	0.99	0.0005	11.79	1.04	0.99	0.2364



**Fig. 15** Fitted kinetic models on experimental methylene blue adsorption data on microporous nanosilica; **a** pseudo-first-order, **b** pseudo-second-order, **c** Intraparticle diffusion (pH 7, adsorbent dosage = 0.4 g/L, room temperature), **d** Possible adsorption mechanisms

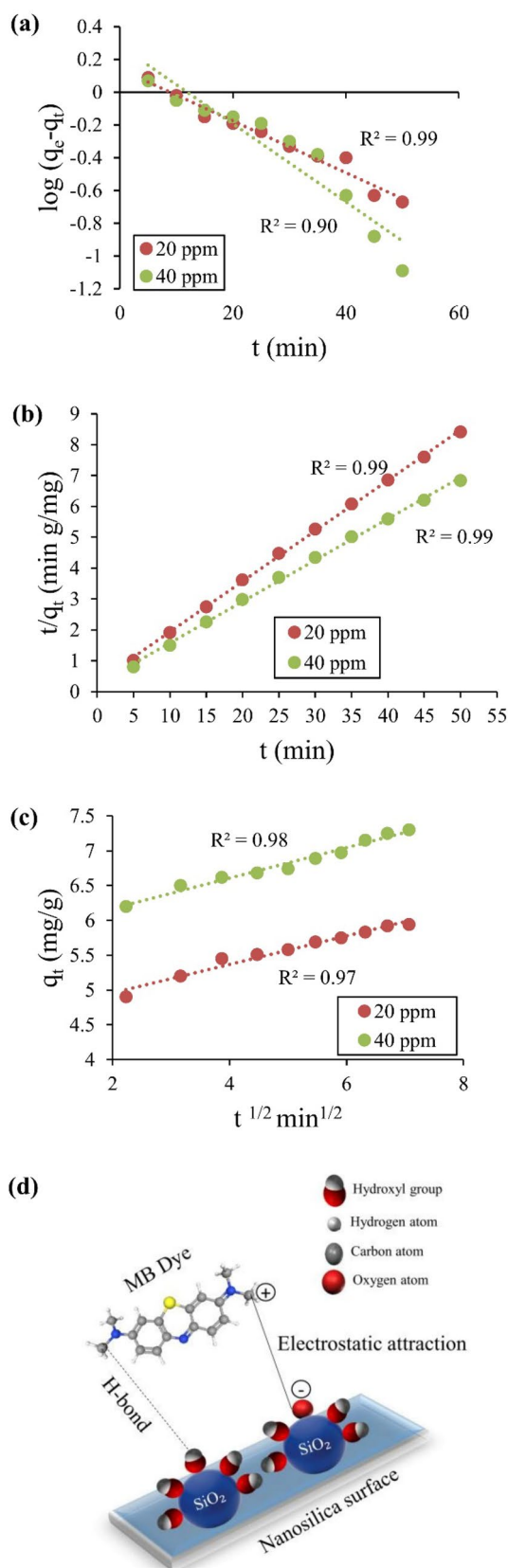
investigation, the  $R_L$  value for all initial concentrations of methylene blue (20 to 100 mg/L) was between 0 and 1, which means the favorable adsorption of methylene blue on the microporous nanosilica. The values of  $K_f = 11.79$  mg/g and  $n = 1.044$  were achieved from the y-intercept and slope of the Freundlich isotherm, respectively. The Freundlich constant,  $n$ , is also known as the adsorption intensity. The value of  $n$  between 1 and 10 represents a favorable adsorption process [46].

### Adsorption Kinetics

Kinetic models are used to fit the experimental data to study the mechanism and rate-controlling steps of the dye adsorption. A deep discernment of adsorption kinetics is critical to building a wastewater treatment system. Adsorption kinetics can also provide helpful information to describe the time required for the adsorption process. Fitting the experimental MB adsorption data by each pseudo-first-order, pseudo-second-order, and intraparticle diffusion models are presented in Fig. 15. The calculated constants and statistical parameters of kinetic models are presented in Table 5. From the constants and statistical parameters in Table 5, it can be clearly seen that the pseudo-second-order model can predict the experimental adsorption data better than the other two kinetic models. This means that chemical adsorption controls the rate of MB adsorption on the porous nanosilica. As illustrated in Fig. 15d, the chemical adsorption occurs through the H-bonding and electrostatic attraction between the nanosilica surface and dye molecules.

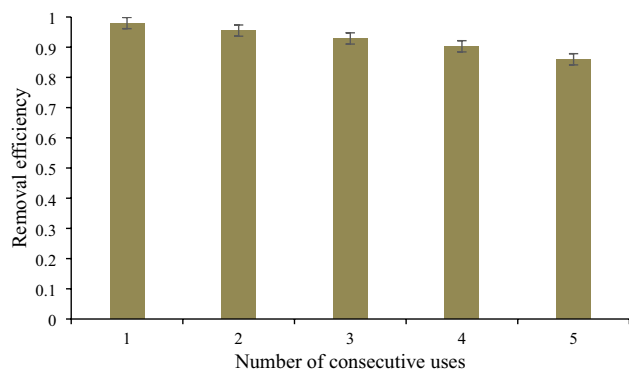
### Reusability Studies

The reusability performance of an adsorbent recreates an irrefutable function in the adsorption process economy and commercial application. Figure 16 displays the reusability results. As it can be observed, the porous nanosilica hydrogel was reused 5 times. The result demonstrated that the porous nanosilica hydrogel exhibited an outstanding reusability until the fourth reuse with removal efficiency of higher than 90%. After the fourth sequential adsorption cycle, the percentage of adsorbed dye decreases to 86%. As shown in Fig. 16, results confirm that the prepared adsorbent could be reused repeatedly without notable destruction of adsorption efficiency. Therefore, reusability experiments without the use of elution agents (such as alkalis, acids, alcohols) for the regeneration treatment indicated that the porous nanosilica can be utilized as an efficient, inexpensive,



**Table 5** Constants and statistical parameters of kinetic models of methylene blue adsorption by microporous nanosilica

Initial methylene blue concentration	Pseudo-first-order kinetic model $\log(q_e - q_t) = \log q_e - kt$				Pseudo-second-order kinetic model $t/q_t = (1/kq_e^2) + (1/q_e)t$				Intraparticle diffusion model $q_t = Kt^{1/2} + C$			
	$R^2$	$k$ (min <sup>-1</sup> )	$q_e$ (mg/g)	$\chi^2$	$R^2$	$k$ (g/mg min)	$q_e$ (mg/g)	$\chi^2$	$R^2$	$K$ (mg/min <sup>1/2</sup> g)	$C$ (mg/g)	$\chi^2$
20 mg/L	0.96	-0.0003	4.15	5.1	0.993	0.088	6.11	0.57	0.97	0.204	4.54	2.53
40 mg/L	0.90	-0.0004	5.32	4.44	0.998	0.076	7.45	0.62	0.97	0.218	5.7	2.25

**Fig. 16** Removal efficiency of methylene blue on the porous nanosilica hydrogel after each reusability cycle (adsorbent dosage = 0.4 g/L, contact time = 60 min, room temperature, concentration = 20 mg/L, pH 7)

and environmentally friendly adsorbent for methylene blue removal from aqueous solutions.

### Comparative Studies

Table 6 provides a comparison between the MB removal performance of the various adsorbents reported and the current porous nanosilica synthesized from the silicomanganese slag. These data clearly show that the MB adsorption capacity of the porous nanosilica developed in this study was much higher than that of other adsorbents recently reported by researchers. It should be noted that studies were selected for comparison that had similar experimental conditions to the current study. Although some adsorbents listed in Table 6 have a higher specific surface area than the porous nanosilica but have lower dye adsorption capacity, this indicates that the porous nanosilica synthesized in this study has a more suitable surface chemistry for the dye adsorption. Also, some adsorbents have shown their best performance in alkaline and acidic pHs, while the adsorbent developed in the current study at pH 7 has the best dye removal performance, which is much better in terms of operational considerations such as equipment corrosion.

### Conclusions and Future Perspectives

This study investigates the adsorption of methylene blue dye from aqueous solutions with concentrations of 20, 50, and 100 mg/L using porous nanosilica obtained from silicomanganese slag. The porous nanosilica was obtained from a facile path based on hydrometallurgy with a high conversion efficiency of silicomanganese slag.

The characterization analyses showed that the amorphous silica obtained had a purity of more than 97%, a specific surface area of 506.14 m<sup>2</sup>/g, a total pore volume of 0.65 cm<sup>3</sup>/g, and an average pore diameter of 10 nm.

Electron microscopy studies disclosed that the nanosilica structure contains round corner particles with a size of 10 to 30 nm, which had formed agglomerates with a size of 50 to 70 nm.

The results of methylene blue dye adsorption experiments revealed that an adsorbent dosage of 0.4 g/L could remove 96 to 98% of methylene blue dye at pH 7 and ambient temperature at all concentrations studied.

A maximum adsorption capacity of 256.41 mg/g was achieved, which was higher than other recently reported adsorbents.

As a general conclusion, the conversion of silicomanganese slag into an effective dye nano-adsorbent can be a promising solution to simultaneously solve the problem of the waste accumulation and environmental problems caused by the release of methylene blue dye.

The performance of the porous nanosilica obtained from silicomanganese slag in water recovery from a real textile wastewater can be investigated in future research. Also, examining the performance of nanosilica obtained from silicomanganese slag in removing other water pollutants is recommended as a future research area. It is also recommended to extract other metal oxides such as Al<sub>2</sub>O<sub>3</sub> and MnO<sub>2</sub> and use them in the process of recovering water from wastewater. Granulation of obtained nanosilica can be studied in order to easily separate it from water after adsorption.



**Table 6** Results of recent research on methylene blue dye removal by other adsorbents

Researcher(s)	Adsorbent	Specific surface area (m <sup>2</sup> /g)	Amount of methylene blue adsorbed (mg/g)	Experimental conditions
The authors of the present work	Microporous nanosilica from silicomanganese slag	474	256.41	T = 25 °C pH 7 Contact time = 60 min Adsorbent dosage: 0.4 g/L Conc. = 20, 50, 100 mg/L
Chandarana et al. [47]	Casuarina equisetifolia pines	–	41.35	T = 303 K pH 7 Contact time = 120 min Adsorbent dosage: 0.5 g/L Conc. = 100 mg/L
Alagarsamy et al. [29]	Biogenic zirconium oxide (ZrO <sub>2</sub> ) nanoparticles	–	23.26	T = 298 K pH 10 Contact time = 300 min Adsorbent dosage: 0.3 g/L Conc. = 20 mg/L
Misran et al. [48]	Banana stem based activated carbon	837.45	101.01	T = ambient temperature pH 7 Contact time = 90 min Adsorbent dosage: 0.2 g/L Conc. = 50 mg/L
Hevira et al. [43]	Terminalia catappa shell	69.88	88.62	T = 298 K pH 5 Contact time = 45 min Adsorbent dosage: 0.1 g/L Conc. = 800 mg/L
Zhang et al. [49]	Coal gasification fine slag residual carbon porous material	574.02	19.18	T = 27 °C pH 8 Contact time = 360 min Adsorbent dosage: 3 g/L Conc. = 50 mg/L
Lu et al. [50]	Nano-structured Fe–Mn binary oxide	67.5	72.32	T = 25 °C pH 7 Contact time = 120 min Adsorbent dosage: 1 g/L Conc. = 100 mg/L
Mouni et al. [22]	Kaolin	21.27	52.76	T = 25 °C pH 6 Contact time = 120 min Adsorbent dosage: 1 g/L Conc. = 100 mg/L
Duman et al. [51]	Agar/κ-carrageenan composite hydrogel	–	242.3	T = 35 °C pH 7 Contact time = 2880 min Adsorbent dosage: – Conc. = 20–40 mg/L
Jiaqi et al. [52]	Carboxyl-functionalized magnetic nanoparticle	–	43.15	T = 25 °C pH 10 Contact time = 120 min Adsorbent dosage: –
Cheng et al. [53]	Salicylic acid–methanol modified steel converter slag	66.665	41.62	T = 293 K pH 7 Contact time = – min Adsorbent dosage: – Conc. = 10–400 mg/L

## Declarations

**Conflict of interest** On behalf of all authors, the corresponding author states that there is no conflict of interest.

## References

- Keller F, Voss RL, Lee RP, Meyer B (2022) Life cycle assessment of global warming potential of feedstock recycling technologies: case study of waste gasification and pyrolysis in an integrated inventory model for waste treatment and chemical production in Germany. *J Resour Conserv Recycl* 179:106106. <https://doi.org/10.1016/j.resconrec.2021.106106>
- Zhang R, Zhang B, Leiviskä T (2022) Vanadium recovery from spent iron sorbent used for the treatment of mining-influenced water. *J Resour Conserv Recycl* 182:106291. <https://doi.org/10.1016/j.resconrec.2022.106291>
- Chen Z, Zheng R, Wei W, Wei W, Zou W, Li J, Ni BJ, Chen H (2022) Recycling spent water treatment adsorbents for efficient electrocatalytic water oxidation reaction. *J Resour Conserv Recycl* 178:106037. <https://doi.org/10.1016/j.resconrec.2021.106037>
- Schwarzenbach RP, Escher BI, Fenner K, Hofstetter TB, Johnson CA, Von Gunten U, Wehrli B (2006) The challenge of micropollutants in aquatic systems. *J Sci* 313:1072–1077. <https://doi.org/10.1126/science.1127291>
- Mashkoo F, Nasar A (2020) Magsorbents: Potential candidates in wastewater treatment technology—a review on the removal of methylene blue dye. *J Magn Magn Mater* 500:166408. <https://doi.org/10.1016/j.jmmm.2020.166408>
- Inamuddin (2019) Xanthan gum/titanium dioxide nanocomposite for photocatalytic degradation of methyl orange dye. *J Int J Biol Macromol* 121:1046–1053. <https://doi.org/10.1016/j.ijbiomac.2018.10.064>
- Cruz-Rizo A, Gutierrez S, Salazar R, Hernández JM (2016) Application of electro-Fenton/BDD process for treating tannery wastewaters with industrial dyes. *Sep Purif Technol*. <https://doi.org/10.1016/j.seppur.2016.08.029>
- Acharya R, Naik B, Parida K (2018) Adsorption of Cr (VI) and textile dyes on to mesoporous silica, titanate nanotubes, and layered double hydroxides. In: ul-Islam S, Butola B (eds) *Nanomaterials in the wet processing of textiles*. Wiley, New York, pp 219–260
- Forgacs E, Cserhati T, Oros G (2004) Removal of synthetic dyes from wastewaters: a review. *J Environ Int* 30:953–971. <https://doi.org/10.1016/j.envint.2004.02.001>
- Shakoor S, Nasar A (2018) Adsorptive decontamination of synthetic wastewater containing crystal violet dye by employing *Terminalia arjuna* sawdust waste. *J Groundw Sustain Dev* 7:30–38. <https://doi.org/10.1016/j.gsd.2018.03.004>
- Chen KC, Wu JY, Liou DJ, Hwang SCJ (2003) Decolorization of the textile dyes by newly isolated bacterial strains. *J Biotechnol* 101:57–68. [https://doi.org/10.1016/S0168-1656\(02\)00303-6](https://doi.org/10.1016/S0168-1656(02)00303-6)
- Robinson T, McMullan G, Marchant R, Nigam P (2001) Remediation of dyes in textile effluent: a critical review on current treatment technologies with a proposed alternative. *J Bioreour Technol* 77:247–255. [https://doi.org/10.1016/S0960-8524\(00\)00080-8](https://doi.org/10.1016/S0960-8524(00)00080-8)
- Papić S, Koprivanac N, Božić AL, Meteš A (2004) Removal of some reactive dyes from synthetic wastewater by combined Al (III) coagulation/carbon adsorption process. *J Dyes Pigm* 62:291–298. [https://doi.org/10.1016/S0143-7208\(03\)00148-7](https://doi.org/10.1016/S0143-7208(03)00148-7)
- El Haddad M, Slimani R, Mamouni R, ElAntri S, Lazar S (2013) Removal of two textile dyes from aqueous solutions onto calcined bones. *J Assoc Arab Univ Basic Appl Sci* 14:51–59. <https://doi.org/10.1016/j.jaubas.2013.03.002>
- Verma M, Dwivedi PK, Saxena SN (2020) Hollow silica nanoparticles synthesized from core-shell nanoparticles as highly efficient adsorbent for methylene blue and its invitro release: mechanism and Kinetics study. *J Colloids Surf A Physicochem Eng Asp* 587:124333. <https://doi.org/10.1016/j.colsurfa.2019.124333>
- Danish M, Ahmad T, Hashim R, Said N, Akhtar MN, Mohamad-Saleh J, Sulaiman O (2018) Comparison of surface properties of wood biomass activated carbons and their application against rhodamine B and methylene blue dye. *J Surf Interfaces* 11:1–13. <https://doi.org/10.1016/j.surf.2018.02.001>
- Zhang Y, Liu J, Du X, Shao W (2019) Preparation of reusable glass hollow fiber membranes and methylene blue adsorption. *J Eur Ceram Soc* 39:4891–4900. <https://doi.org/10.1016/j.jeureram.2019.06.038>
- Supelano G, Cuaspid JG, Moreno-Aldana LC, Ortiz C, Trujillo C, Palacio C, Vargas CAP, Gómez JAM (2020) Synthesis of magnetic zeolites from recycled fly ash for adsorption of methylene blue. *Fuel* 263:116800. <https://doi.org/10.1016/j.fuel.2019.116800>
- Shooto ND, Nkutha CS, Guilande NR, Naidoo EB (2020) Pristine and modified mucuna beans adsorptive studies of toxic lead ions and methylene blue dye from aqueous solution. *J S Afr J Chem Eng* 31:33–43. <https://doi.org/10.1016/j.sajce.2019.12.001>
- Ahmad A, Khan N, Giri BS, Chowdhary P, Chaturvedi P (2020) Removal of methylene blue dye using rice husk, cow dung and sludge biochar: characterization, application, and kinetic studies. *J Bioreour Technol* 306:123202. <https://doi.org/10.1016/j.biortech.2020.123202>
- Adel M, Ahmed MA, Mohamed AA (2021) Synthesis and characterization of magnetically separable and recyclable crumbled  $MgFe_2O_4$ /reduced graphene oxide nanoparticles for removal of methylene blue dye from aqueous solutions. *J Phys Chem Solids* 149:109760. <https://doi.org/10.1016/j.jpcs.2020.109760>
- Mouni L, Belkhir L, Bollinger JC, Bouzaza A, Assadi A, Tirri A, Dahmoune F, Madani K, Remini H (2018) Removal of Methylene Blue from aqueous solutions by adsorption on Kaolin: kinetic and equilibrium studies. *J Appl Clay Sci* 153:38–45. <https://doi.org/10.1016/j.clay.2017.11.034>
- Ye J, Dieudonne N, Tang B, Bin L, Li P, Huang S, Fu F, Cai Y, Guan G, Hao X (2020) Facilely synthesized recyclable mesoporous magnetic silica composite for highly efficient and fast adsorption of Methylene Blue from wastewater: thermodynamic mechanism and kinetics study. *J Mol Liq* 303:112656. <https://doi.org/10.1016/j.molliq.2020.112656>
- Jiang X, Zhang H, Yue M, Zhang S, Li Y, Xu W (2019) Synthesis of organic hybrid super-microporous silicas as an adsorbent for dyes removal from water. *J Microporous Mesoporous Mater* 288:109598. <https://doi.org/10.1016/j.micromeso.2019.109598>
- Tan CHC, Sabar S, Hussin MH (2018) Development of immobilized microcrystalline cellulose as an effective adsorbent for methylene blue dye removal. *J S Afr J Chem Eng* 26:11–24. <https://doi.org/10.1016/j.sajce.2018.08.001>
- Miyah Y, Lahrachi A, Idrissi M, Khalil A, Zerrouq F (2018) Adsorption of methylene blue dye from aqueous solutions onto walnut shells powder: equilibrium and kinetic studies. *J Surf Interfaces* 11:74–81. <https://doi.org/10.1016/j.surf.2018.03.006>
- Ibupoto AS, Qureshi UA, Ahmed F, Khatri Z, Khatri M, Maqsood M, Brohi RZ, Kim IS (2018) Reusable carbon nanofibers for efficient removal of methylene blue from aqueous solution. *J Chem Eng Res Des* 136:744–752. <https://doi.org/10.1016/j.cherd.2018.06.035>
- Beagana A, Alotaibi K, Almakhlafi M, Algarabli W, Alajmi N, Alanazi M, Hajer A, Alharbi F, Alshammari R, Alswieleh A (2022) Amine and sulfonic acid functionalized mesoporous silica as an effective adsorbent for removal of methylene blue from contaminated water. *J King Saud Univ Sci* 34:101762. <https://doi.org/10.1016/j.jksus.2021.101762>

29. Alagarsamy A, Chandrasekaran S, Manikandan A (2022) Green synthesis and characterization studies of biogenic zirconium oxide (ZrO<sub>2</sub>) nanoparticles for adsorptive removal of methylene blue dye. *J Mol Struct* 1247:131275. <https://doi.org/10.1016/j.molstruc.2021.131275>
30. Hosseini H, Zirakjou A, JulianMcClements D, Goodarzi V, Chen WH (2022) Removal of methylene blue from wastewater using ternary nanocomposite aerogel systems: carboxymethyl cellulose grafted by polyacrylic acid and decorated with graphene oxide. *J Hazard Mater* 421:126752. <https://doi.org/10.1016/j.jhazmat.2021.126752>
31. Allahverdi A, Ahmadnezhad S (2014) Mechanical activation of silicomanganese slag and its influence on the properties of Portland slag cement. *Powder Technol* 251:41–51. <https://doi.org/10.1016/j.powtec.2013.10.023>
32. Aragaw TA (2020) Recovery of iron hydroxides from electrocoagulated sludge for adsorption removals of dye wastewater: adsorption capacity and adsorbent characteristics. *J Surf Interfaces* 18:100439. <https://doi.org/10.1016/j.surfint.2020.100439>
33. Bo L, Gao F, Bao S, Bian Y, Liu Z, Da Y (2021) A novel adsorbent Auricularia Auricular for the removal of methylene blue from aqueous solution: isotherm and kinetics studies. *Environ Technol Innov* 23:101576. <https://doi.org/10.1016/j.eti.2021.101576>
34. Bello M, Abdus-Salam N, Adekola AF, Pal U (2021) Isotherm and kinetic studies of adsorption of methylene blue using activated carbon from ackee apple pods. *Chem Data Collect* 31:100607. <https://doi.org/10.1016/j.cdc.2020.100607>
35. TubaGemici B, UcuOzel H, BarisOzel H (2021) Removal of methylene blue onto forest wastes: adsorption isotherms, kinetics and thermodynamic analysis. *Environ Technol Innov* 22:101501. <https://doi.org/10.1016/j.eti.2021.101501>
36. Namvar M, Mahinroosta M, Allahverdi A (2021) Highly efficient green synthesis of highly pure microporous nanosilica from silicomanganese slag. *J Ceram Int* 47:2222–2229. <https://doi.org/10.1016/j.ceramint.2020.09.062>
37. Ahmad MA, Rahman NK (2011) Equilibrium, kinetics and thermodynamic of Remazol Brilliant Orange 3R dye adsorption on coffee husk-based activated carbon. *Chem Eng J* 170:154–161. <https://doi.org/10.1016/j.cej.2011.03.045>
38. Hurairah SN, Lajis NM, Halim AA (2020) Methylene blue removal from aqueous solution by adsorption on *Archidendron jiringa* seed shells. *J Geosci Environ Prot* 8:128–143. <https://doi.org/10.4236/gep.2020.82009>
39. Lata H, Garg VK, Gupta RK (2007) Removal of a basic dye from aqueous solution by adsorption using *Parthenium hysterophorus*: an agricultural waste. *J Dyes Pigment* 74:653–658. <https://doi.org/10.1016/j.dyepig.2006.04.007>
40. Aksakal O, Ucu H (2010) Equilibrium, kinetic and thermodynamic studies of the biosorption of textile dye (Reactive Red 195) onto *Pinus sylvestris* L. *J Hazard Mater* 181:666–672. <https://doi.org/10.1016/j.jhazmat.2010.05.064>
41. Lu P, Hsieh YL (2012) Highly pure amorphous silica nano-disks from rice straw. *J Powder Technol* 225:149–155. <https://doi.org/10.1016/j.powtec.2012.04.002>
42. Mourhly A, Jhilal F, El Hamidi A, Halim M, Arsalane S (2019) Highly efficient production of mesoporous nano-silica from unconventional resource: process optimization using a central composite design. *Microchem J* 145:139–145. <https://doi.org/10.1016/j.microc.2018.10.030>
43. Hevira L, Ighalo JO, Aziz H, Zein R (2021) Terminalia catappa shell as low-cost biosorbent for the removal of methylene blue from aqueous solutions. *J Ind Eng Chem* 97:188–199. <https://doi.org/10.1016/j.jiec.2021.01.028>
44. Sartape AS, Mandhare AM, Jadhav VV, Raut PD, Anuse MA, Kolekar SS (2017) Removal of malachite green dye from aqueous solution with adsorption technique using *Limonia acidissima* (wood apple) shell as low cost adsorbent. *J Arab J Chem* 10:S3229–S3238. <https://doi.org/10.1016/j.arabjc.2013.12.019>
45. Gimbert F, Morin-Crini N, Renault F, Badot P-M, Crini G (2008) Adsorption isotherm models for dye removal by cationized starch-based material in a single component system: error analysis. *J Hazard Mater* 157:34–46. <https://doi.org/10.1016/j.jhazmat.2007.12.072>
46. Mittal A, Kurup L, Mittal J (2007) Freundlich and Langmuir adsorption isotherms and kinetics for the removal of Tartrazine from aqueous solutions using hen feathers. *J Hazard Mater* 146:243–248. <https://doi.org/10.1016/j.jhazmat.2006.12.012>
47. Chandarana H, Kumar PS, Seenuvasan M, Kumar MA (2021) Kinetics, equilibrium and thermodynamic investigations of methylene blue dye removal using *Casuarina equisetifolia* pines. *J Chemosphere* 285:131480. <https://doi.org/10.1016/j.chemosphere.2021.131480>
48. Mirsan E, Bani O, Situmeang EM, Purba AS (2022) Banana stem based activated carbon as a low-cost adsorbent for methylene blue removal: Isotherm, kinetics, and reusability. *J Alex Eng J* 61:1946–1955. <https://doi.org/10.1016/j.aej.2021.07.022>
49. Zhang Y, Wang R, Qiu G, Jia W, Guo Y, Guo F, Wu J (2021) Synthesis of porous material from coal gasification fine slag residual carbon and its application in removal of methylene blue. *J Mol* 26:6116. <https://doi.org/10.3390/molecules26206116>
50. Lu K, Wang T, Zhai L, Wu W, Dong S, Gao S, Mao L (2019) Adsorption behavior and mechanism of Fe-Mn binary oxide nanoparticles: adsorption of methylene blue. *J Colloid Interface Sci* 539:553–562. <https://doi.org/10.1016/j.jcis.2018.12.094>
51. Duman O, Polat TG, Diker CÖ, Tunç S (2020) Agar/k-carrageenan composite hydrogel adsorbent for the removal of methylene blue from water. *J Int J Biol Macromol* 160:823–835. <https://doi.org/10.1016/j.jbiomac.2020.05.191>
52. Jiaqi Z, Yimin D, Danyang L, Shengyun W, Liling Z, Yi Z (2019) Synthesis of carboxyl-functionalized magnetic nanoparticle for the removal of methylene blue. *J Colloids Surf A: Physicochem Eng Asp* 572:58–66. <https://doi.org/10.1016/j.colsurfa.2019.03.095>
53. Cheng M, Zeng G, Huang D, Lai C, Liu Y, Zhang C, Wang R, Qin L, Xue W, Song B (2018) High adsorption of methylene blue by salicylic acid-methanol modified steel converter slag and evaluation of its mechanism. *J Colloid Interface Sci* 515:232–239. <https://doi.org/10.1016/j.jcis.2018.01.008>

**Publisher's Note** Springer Nature remains neutral with regard to jurisdictional claims in published maps and institutional affiliations.

Springer Nature or its licensor (e.g. a society or other partner) holds exclusive rights to this article under a publishing agreement with the author(s) or other rightsholder(s); author self-archiving of the accepted manuscript version of this article is solely governed by the terms of such publishing agreement and applicable law.